ELSEVIER

Earth and Planetary Science Letters 140 (1996) 83–96

EPSL

Seismic anisotropy beneath Tibet: evidence for eastward extrusion of the Tibetan lithosphere?

J. Lavé [a,*], J.P. Avouac [a], R. Lacassin [b], P. Tapponnier [b], J.P. Montagner [b]

[a] *Laboratoire de Géophysique, CEA, BP. 12, 91680 Bruyères-Le-Châtel, France*
[b] *Institut de Physique du Globe, 4 Place Jussieu, 75230 Paris Cédex 05, France*

Received 19 May 1995; accepted 28 February 1996

Abstract

Strong seismic anisotropy beneath Tibet has recently been reported from the study of SKS shear wave splitting. The fast split waves are generally polarized in an easterly direction, close to the present day direction of motion of the Tibetan crust relative to stable Eurasia, as deduced from Holocene slip rates on the major active faults in and around Tibet. This correlation may be taken to suggest that the whole Tibetan lithosphere is being extruded in front of indenting India and that the anisotropic layer is the deforming asthenosphere, that accommodates the motion of the Tibetan lithosphere relative to the fixed mantle at depth. Uncertainties about this motion are at present too large to bring unambiguous support to that view. Assuming that this view is correct however, a simple forward model is used to compute theoretical delay times as a function of the thickness of the anisotropic layer. The observed delay times would require a 50–100 km thick anisotropic layer beneath south-central Tibet and an over 200 km thick layer beneath north-central Tibet, where particularly hot asthenosphere has been inferred. This study suggests that the asthenospheric anisotropy due to present absolute block motion might be dominant under actively deforming continents.

Keywords: Tibet; SKS-waves; time variations; lithosphere; Neotectonics

1. Introduction

Recent measurements of SKS waves at several stations on the Tibetan plateau have revealed particularly strong seismic anisotropy [1–3]. The reported delay times of 1–2.5 s between split waves range among the largest values ever observed [4–8]. Seismic anisotropy is usually attributed to strain-induced preferred orientation of minerals in the ductile part of the lithosphere, or to crack distribution within the brittle crust, and may therefore help to unravel tectonic processes at depth.

In continental areas, strong anisotropy is often observed below cratonic shields, where it is generally interpreted as due to frozen fabrics related to past tectonics [7,9]. The interpretation of these data is often difficult because old tectonic events and plate motions cannot be tightly constrained. By contrast, in areas of active tectonics, such as the Tibetan Plateau, the correlation between tectonics and seismic anisotropy could be tested in a more quantitative way. McNamara et al. [1] pointed out the correspondence between the fast polarization directions (FPD)

* Corresponding author. E-mail: lave@ldg.bryeres.cea.fr

PII S0012-821X(96)00045-3

and the roughly E–W trend of geological structures. They concluded that there must be some correlation between strains in the mantle and the extrusion pattern, as expressed in the surface geology. Moreover, as noted by Hirn et al. [2] and Guilbert et al. [3], FPD make a pattern similar to the velocity field describing the present motion of Tibet with respect to stable Eurasia (Fig. 1). It might suggest that, as beneath oceans [10,11], the source of anisotropy might be a decoupling layer accommodating the displacement of the lithospheric blocks with respect to the deep mantle.

Crustal anisotropy cannot produce delay times of more than a few 1/10 of a second [12]. In fact, Herquel et al. [13] have found a crustal anisotropy beneath northern Tibet that is roughly parallel to SKS anisotropy, but with delay times of about 0.2–0.3 s at most. On the other hand, rocks of the deep mantle (below the phase transition at 410 km) are only weakly anisotropic [7,14,15]. The most proba-

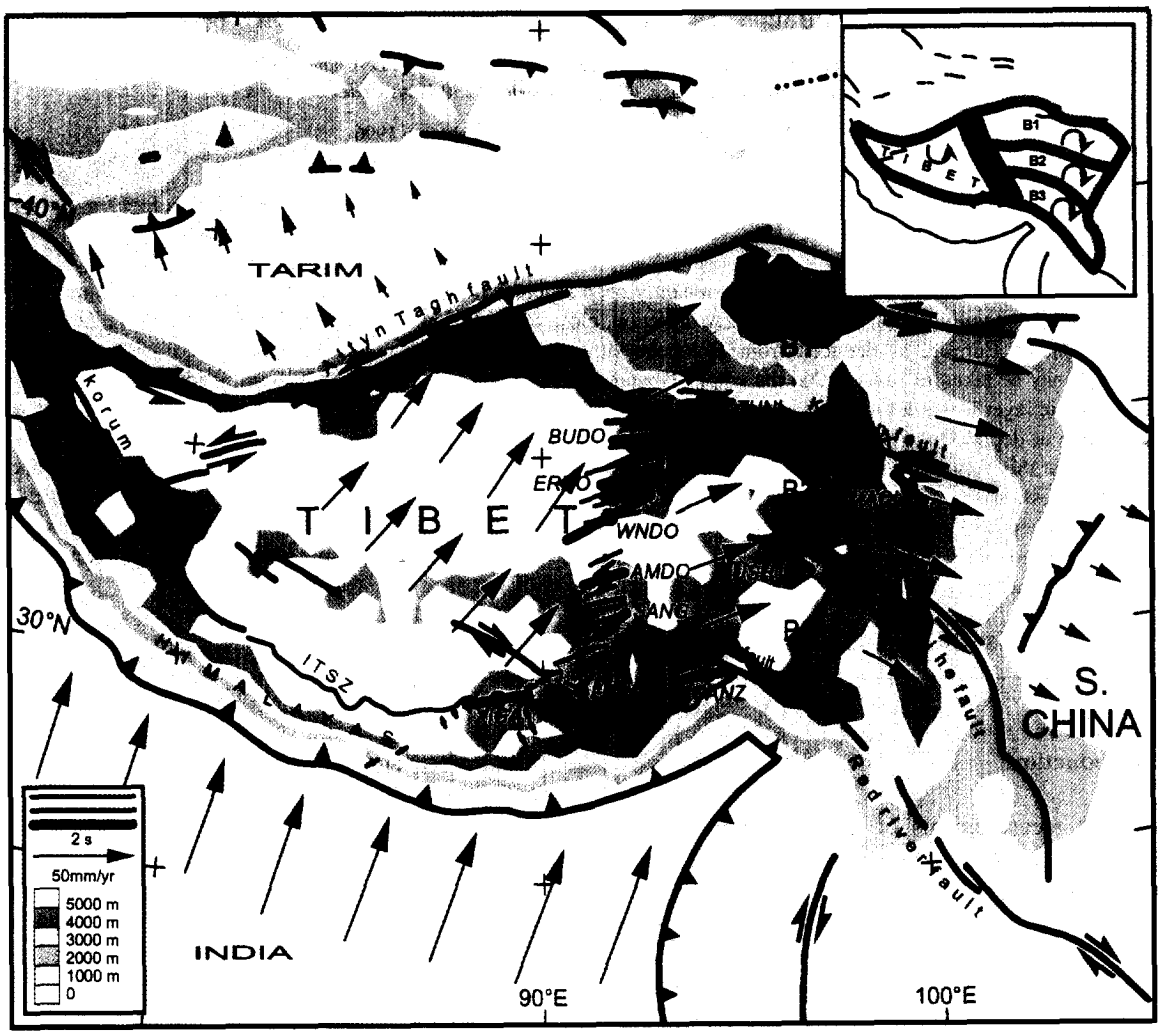

Fig. 1. Velocity field describing motions (red arrows) relative to Siberia, derived from Holocene slip-rates on major faults in central Asia [28]. Mean direction of polarization of fast split waves are also reported from McNamara et al. [1] (thick blue bars), Hirn et al. [2] (pink bars) and Guilbert et al. [3] (light blue bars). Length of each bar is proportionnal to the mean delay time between fast and slow split waves. ITSZ = Indus–Tsangpo Suture Zone.

ble source of anisotropy is, therefore, the upper mantle, where it is thought to reflect the Lattice Preferred Orientation (LPO) of olivine minerals (e.g., [16,17]). The LPO of olivine in deformed peridotite results from ductile shear that forms foliation planes close to the shear plane and stretching lineations marking the shear direction. As a convention, let X be the direction of the stretching lineation, Y the direction normal to the lineation in the foliation plane, and Z the direction normal to the foliation plane. In peridotite the fastest S waves are propagating along Y and are polarized along X [14]. For S waves propagating either along Z (normal to the foliation), or along X (parallel to the lineation), the birefringence is about half that observed for S waves propagating along Y. The polarized, fast S waves lie parallel to the lineation direction and in the foliation plane. This scheme provides the basis for the interpretation of seismic anisotropy in terms of upper mantle deformation.

In the following, we first overview recent observations of seismic anisotropy beneath Tibet. We describe current models of lithospheric deformation of Asia and discuss their implications with respect to seismic anisotropy. A model of rigid lithospheric block tectonics is shown to be consistent with the apparent correlation of FPD with direction of present tectonic transport but uncertainties are still too large to bring unambiguous support to that view. We finally investigate the implications of such a model by comparing observed delay times with theoretical values derived from a simple forward calculation.

2. Seismic anisotropy beneath Tibet

2.1. Overview of recent observations

Three experiments have recently provided information on seismic anisotropy beneath Tibet. McNamara et al. [1] operated 11 broad-band stations for 1 year. They recorded numerous SKS with evidence for shear wave splitting at 7 stations (Fig. 1). Hirn et al. [2] and Guilbert et al. [3] used short-period stations in Nepal and Tibet (Fig. 1). Few SKS waves were recorded during these experiments. Observations of shear wave splitting of S and ScS waves were also described by Guilbert et al. [3]. Given that the data are few and that shear wave splitting is known to be sensitive to incidence and back azimuth, especially if several anisotropic layers are involved [8], some variability in the observations was to be expected. Where they overlap, the three experiments yield FPD that differ at most by 20° and generally by less than 10° (Figs. 1 and 3). Delay times are more variable. For example, at BUDO, McNamara et al. [1] obtained a delay time of 2.4 s while Guilbert et al. [3] reported 1.1 s. Such a variability is in keeping with the observation that independent determinations at a given station can yield delay times varying within a factor 2 [1]. Altogether, the three experiments attest for particularly strong seismic anisotropy with the following characteristics:

(1) From the Lesser Himalaya to the Indus–Tsangpo Suture Zone (ITSZ) the anisotropy is weak.

(2) The anisotropy is stronger in central Tibet, north of the ITSZ, with delay times of the order of 1 s and northeast-trending FPD.

(3) The anisotropy is strongest beneath North Central Tibet, close to the Kunlun fault, with delay times between 1 s and 2.5 s. The FPD rotates rapidly in this area and tends to be parallel to the Kunlun fault.

In the following we mostly refer to the results of McNamara et al. [1], because their experiment provided numerous measurements with various back azimuths, allowing for better constrained estimates of average delay times and uncertainties. However, we check azimuthal consistency with the more recently published data of Hirn et al. [2] and Guilbert et al. [3].

2.2. Seismic anisotropy and mantle deformation beneath Tibet

The indentation of India into Asia has induced large scale strike-slip and thrust faulting, allowing for both crustal thickening and lateral extrusion (e.g., [18,19]). Two competing views of lithospheric mantle deformation beneath Tibet are presently advocated, and rely on different appreciation of the mechanical significance of the strike-slip faults in and around Tibet. One view is that deformation tends to localize along a few large shear zones (e.g., [20]),

while the other assumes more homogeneously distributed strain in the strong upper mantle part of the lithosphere (e.g., [21]).

2.2.1. Homogeneous thickening of the lithosphere

England and Molnar [22] have argued that the strike-slip faults are limited to the upper crust and chiefly accommodate the vorticity of mantle deformation at depth. The mantle would absorb the convergence between India and Asia by homogeneous thickening, so that a dominant lithospheric anisotropy should be expected. Vertical foliation planes perpendicular to the N20°E convergence between India and Eurasia [23] should develop at the front of the indentor. The observed FPD differ generally by more than 30–40° from the N110°E direction expected. In addition, such a model cannot explain why the anisotropy might get stronger to the north, away from the indentor. It has also been proposed that, in response to homogeneous thickening of the cold, gravitationally unstable, upper mantle, the lower part of the lithosphere may have sunk into the deep mantle [24]. Had this process occurred beneath Tibet (e.g., [25]), we would expect little correlation between crustal deformation and seismic anisotropy [1]. The arguments for discarding models of homogeneous deformation of the lithosphere are weak, but since a more quantitative assessment of the predictions of these models regarding seismic anisotropy is not an easy task, we only examine below to what extent the observed anisotropy can be considered consistent with a lithospheric blocks model.

2.2.2. Rigid lithospheric blocks

The major strike-slip faults in and around Tibet, such as the Altyn Tagh, the Kunlun or the Karakorum faults, might be lithospheric shear zones allowing for lateral extrusion of the Tibetan lithosphere [20]. Such a view implies localized vertical shear along the major fault zones and horizontal decou-

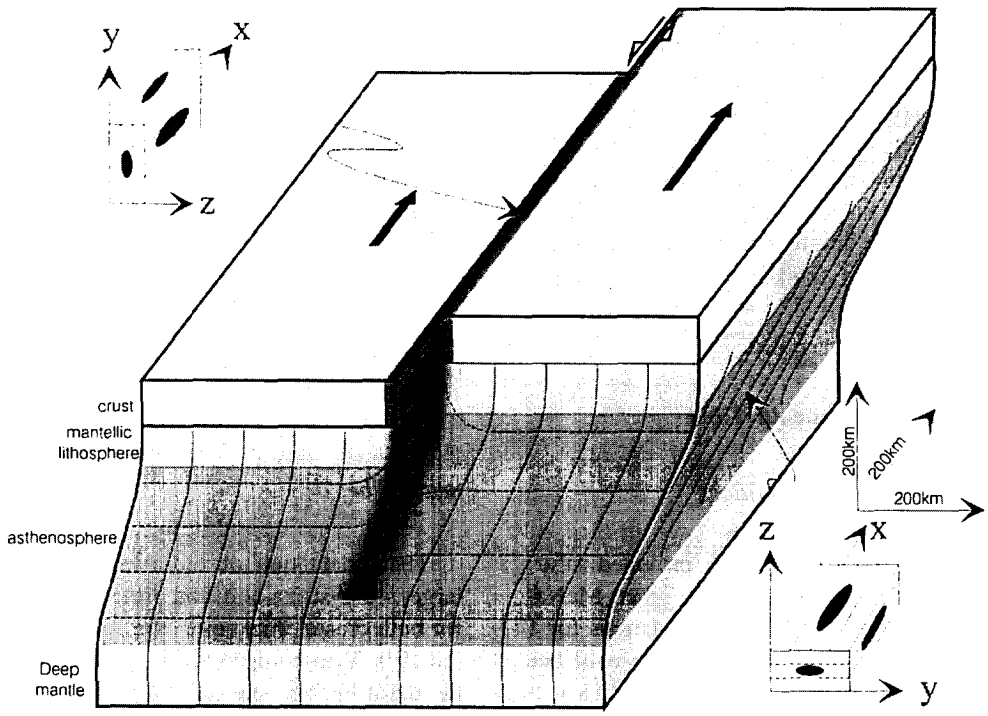

Fig. 2. Lithospheric and asthenospheric deformation predicted by the lithospheric block model. Shear zones are indicated in medium gray to dark gray shading. Deformation within lithosphere is assumed to be localized along major faults zones. Strike-slip faulting tends to produce vertical foliation planes parallel to the fault strike, with horizontal stretching lineations. Shear below lithosphere would yield nearly horizontal foliation planes, with stretching lineations parallel to direction of motion of the lithosphere relative to deep mantle.

pling between the lithosphere and the deep mantle (Fig. 2). Two sources of anisotropy should therefore result. Lithospheric deformation within and near the active fault zones should favour fault-parallel FPD. Anisotropy due to shear at the base of the lithosphere should tend polarize the fast SKS split waves along the direction of tectonic transport with respect to the mantle. Although nearly horizontal foliation in the deforming asthenosphere is not the most favourable case for splitting of nearly vertical incident S waves, this configuration can lead to significant SKS shear wave splitting [26]. At stations lying close to major strike-slip faults, such as BUDO and TUNL on the Kunlun fault, or USHU on the Xianshuihe fault, the observed polarization directions tend to be parallel to the strike of the faults, suggesting that such faults reach deep into the crust and mantle, leading to a dominant lithospheric anisotropy. On the other hand, the apparent correlation of directions of tectonic transport with FPD at the stations located away from the major fault zones, such as SANG, AMDO, WNDO, ERDO and MAQI, suggests a dominant sublithospheric anisotropy.

Seismic anisotropy beneath Tibet seems therefore more consistent with lithospheric block tectonics than with homogeneous thickening. Hereafter we investigate this possibility more quantitatively and try to infer the thickness of the asthenospheric anisotropic zone and the eventual contribution of the lithospheric anisotropy from the observed delay times.

3. Comparison between fast S wave polarization and present motion of the lithosphere

A quantitative assessment of the apparent correlation shown in Fig. 1 requires determination of directions of tectonic transport with respect to the deep mantle, computed at the location of the seismic stations.

3.1. Kinematics of active deformation in central and eastern Tibet

The kinematics of active crustal deformation in central Asia have been derived from the estimates of Holocene slip rates on some of the major faults of Asia [20,27,28]. The available data appear to be consistent with a lithospheric block model in which the major fault zones are considered to be separate, rigid, rotating blocks [28]. This model considers four rotating blocks (Siberia, Tarim, Tibet and India) on a spherical earth. The Eulerian poles describing the motion of these blocks (Table 1) have been obtained from the inversion of the slip rates on the major faults. The corresponding velocity field, with respect to stable Eurasia, is shown in Fig. 1. The velocity field has been extrapolated in eastern Tibet on the basis of a simple geometrical model, in which rotation of blocks B1, B2 and B3 (Fig. 1) transfers the northeastward extrusion of central Tibet into an eastward extrusion of south China [28]. The Euler pole of the Qaidam block, B1, was computed assuming that this block rotates at about 1°/my, as suggested from the gradient of crustal shortening along the Nan Shan [29]. The other poles (Table 1) have been deduced from fault geometries and assuming about 1 cm/yr of left-lateral slip on the Kunlun and Xianshuihe faults [30,31]. Before any quantitative comparison with seismic anisotropy, one must bear in mind that the uncertainties on the azimuth of seismic anisotropy are of the order of 10° (this value was estimated from the distribution of independent measurements at the same station [1]), and that the uncertainties on the kinematic model are large as well. First, the uncertainty about the motion of India with respect to Eurasia has been ignored by Avouac and Tapponnier [28]. Second, a small amount of strain is probably taken up by minor faults not considered in the model. Third, slip rates have been estimated from the offsets of geomorphological markers, which are generally not precisely dated.

Table 1
Euler vectors describing crustal deformation in Central Asia in terms of rigid lithospheric blocks (from [28])

Block	Latitude (°N)	Longitude (°N)	ω (°/Ma)
Tibet	44.2	64.4	0.89
B1	23.2	101.8	1.00
B2	24.3	100.5	1.37
B3	25.8	98.7	2.15

The Eurasian plate is considered as fixed and counter-clockwise rotations are taken to be positive.

Altogether, at points on the central Tibetan block, the uncertainties on the velocities are about 20–30% in magnitude and 30° in azimuth (at the 1σ confidence level). The motion of the blocks in eastern Tibet is less well constrained, so that uncertainties on velocities are probably still larger. In southern Tibet the oblique convergence between India and central Tibet is partitioned between roughly pure thrust along the Himalaya, right-lateral strike slip faulting along KJFZ, and normal faulting on the north–south striking south Tibetan rifts [27]. The implications for mantle deformation of such a complex tectonic setting are not straightforward. This is why we do not consider, in this paper, the seismic anisotropy observed in southern Tibet (in particular, at stations XIGA, LHSA and GANZ).

3.2. Rate and direction of tectonic transport at the seismic stations

In order to assess the correspondence between the azimuths of the velocity vectors, ϕ_t, and of FPD, ϕ_s, the velocities, v_i, predicted by the kinematic model of Avouac and Tapponnier [28] have been computed at the locations of the stations of McNamara et al. [1] (Table 2). Four seismic stations lie well within some of the Tibetan blocks: TUNL lies on the Tsaïdam block (B1), BUDO and MAQI on the block between Kunlun and Xianshuihe faults (B2), and USHU on the block south of Xianshuihe fault (B3). The four other stations, SANG, AMDO, ERDO and WNDO, lie between central Tibet and the rotating blocks in eastern Tibet. For each of these 4 points, we averaged the two vectors computed with the Euler poles of central Tibet or of the adjacent block to the east. The two vectors are generally close, since the displacement field between central Tibet and eastern Tibet is approximately continuous, as required by the absence of large faults in this area.

The histogram of the difference of azimuths, $\Delta\phi = \phi_s - \phi_t$, is relatively narrow, with a variance $\sigma(\Delta\phi) = 10°$ (Fig. 3A). Compared to the plate velocities computed relative to stable Eurasia, the FPD lie systematically about $\Delta\phi = 29°$E, on average to the east (Fig. 3A). Given that uncertainties on azimuths ϕ_s and ϕ_t are of the order of 10° and 30°, respectively, the small standard deviation $\sigma(\Delta\phi) = 10°$ implies that some correlation between the two patterns exists. This correlation pattern is well corroborated by the differences in azimuths derived from the FPD observed by Hirn et al. [2] and by Guilbert et al. [3] (Fig. 3B and C, respectively), which yield respectively $\Delta\phi = 30°$E and 28°E, on average, and standard deviations $\sigma(\Delta\phi) = 7.5°$ and 11.5°. The fairly large difference in azimuths ($\Delta\phi =$ 29°E, on average) may be taken to indicate some systematic bias. This bias could be due to the fact that the Eurasian plate should not be considered fixed with respect to the deep mantle beneath Tibet. Unfortunately, the absolute plate motion (APM) of Eurasia with respect to the deep fixed mantle is poorly constrained. NNR-Nuvel 1 [32] would imply a motion, relative to deep mantle, of a point in central Tibet attached to Eurasia at nearly 2.6 cm/yr

Table 2
Comparison between seismic anisotropy and present tectonic transport

seismic station	lithospheric block	seismic anisotropy (*)		velocity / stable Eurasia (**)	
		ϕ_S (°E)	δt (s)	ϕ_t (°E)	v (cm/yr)
AMDO	Tibet - B3	75.0	0.88	41	3.9
BUDO	B2	86.7	2.40	61	3.4
ERDO	Tibet - B2	73.4	1.49	44	3.7
SANG	Tibet - B3	51.0	0.80	39	3.8
TUNL	B1	88.8	0.93	63	2.8
WNDO	Tibet - B2	62.0	1.91	42	3.8
MAQI	B2	131.8	0.82	89	2.7
USHU	B3	119.0	0.72	78	3.1

* Anisotropy parameters from McNamara et al. [1].
** Present velocities relative to Eurasia derived from [28].

towards the east-southeast (Fig. 4). A model derived from 7 Pacific hot spots, HS-Nuvel 1 [33] implies 1 cm/yr to the west-northwest. Another solution, derived from the trend of 14 hot spot chains, HST-Nuvel 1 [34], implies 1 cm/yr to the southeast. Given the great differences between the 3 APM determinations, we have explored the space of all possible motions of less than 3 cm/yr (Fig. 4). At all the stations the same velocity correction was applied, an assumption that requires the Eurasian APM Euler pole to lie far from Tibet. For each value, $\Delta\phi$ and $\sigma(\Delta\phi)$ were computed (Fig. 4). For NNR-Nuvel 1 and HST-Nuvel 1 the systematic bias on $\Delta\phi$ are 8°E and 15°E, respectively, while the standard deviations, $\sigma(\Delta\phi)$, are 15° and 11°, respectively (Fig. 3). These two APM would, therefore, imply a slightly better fit between ϕ_s and ϕ_t, than that obtained by assuming no motion of the Eurasian plate with respect to the deep mantle below Tibet. HS-Nuvel 1 yields a larger misfit, $\Delta\phi = 45$°E, with a slightly better standard deviation $\sigma(\Delta\phi) < 10$°. The best correlation between ϕ_s and ϕ_t would be obtained with 2 cm/yr of northward motion of the mantle beneath Tibet with respect to the Eurasian plate. Given the large uncertainties on crustal tectonics and on fast S wave polarization azimuths, it appears that whatever south to eastward APM solution is considered, the azimuths of the FPD and the directions of tectonic transport can be considered to correlate, but this correlation cannot be considered as a strong positive test.

4. Discussion of delay times: a simple forward model

In this section we assume that the dominant anisotropic layer, away from the major faults zones, is the sheared asthenosphere accommodating the relative motion between the extruded lithosphere of Tibet and a fixed mantle at depth. The delay time, δt, resulting from an anisotropic layer with thickness H is:

$$\delta t = ks^* H/Vs \quad \text{with} \quad ks = \Delta Vs/Vs \qquad (1)$$

where Vs is the mean shear wave velocity, and ΔVs is the difference in shear wave velocity for waves polarized along the fast and slow directions, respectively. Delay times thus depend on the thickness of the anisotropic layer, H, and on the birefringence, ks. These quantities are not independent, since strain, hence seismic anisotropy, in the decoupling layer

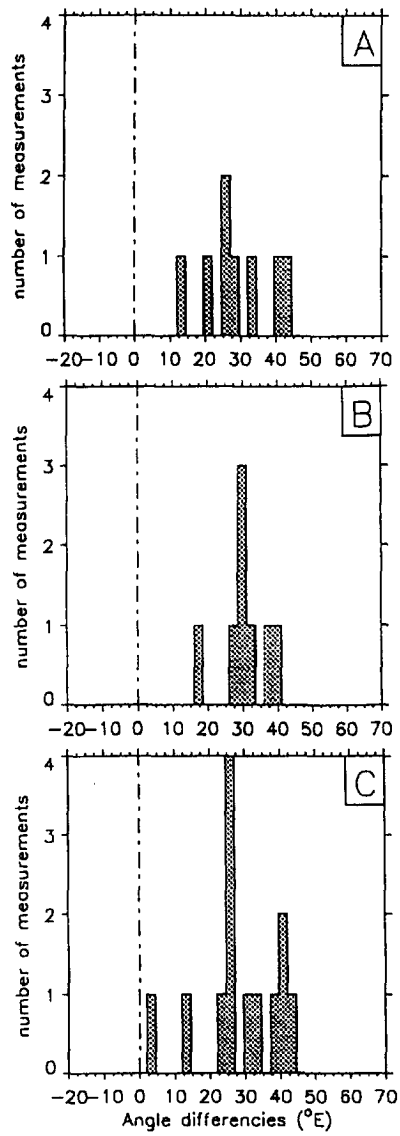

Fig. 3. Histogram of azimuth differences, $\Delta\phi = \phi_s - \phi_t$, predicted by the kinematic model of Avouac and Tapponnier [28] computed at the locations of the stations of McNamara et al. [1]s − ϕt, between the Fast Polarization Direction (FPD) of SKS split waves, ϕ_s, and the direction of motion of the lithosphere relative to stable Eurasia, ϕ_t. (A) FPD reported by McNamara et al. [1]; (B) FPD of Hirn et al. [2]; (C) FPD of Guilbert et al. [3].

depends on its thickness. A forward computation of delay times therefore requires laws to convert the displacement of the lithosphere with respect to the deep mantle into finite shear strain, then into olivine crystal LPO and, finally, into seismic anisotropy.

4.1. Strain in the asthenosphere

If the observed anisotropy results from the penetrative fabric of deformed rocks, it should be interpreted in terms of finite strain rather than in terms of instantaneous strain rate. Assuming that any initial LPO in the upper mantle is rapidly annealed, anisotropy in the decoupling layer at base of the lithosphere depends essentially on the finite displacement of the lithosphere with respect to the deep mantle. Assuming a constant low viscosity in this layer, the shear strain, γ, would be directly proportional to the total relative displacement between the lithosphere and the asthenosphere, L:

$$\gamma = L/H \tag{2}$$

Geological evidence suggests that the present tectonic regime began 15–17 my ago (e.g., [35,36]). Assuming that the velocity field has been stationary since that time, the finite displacement between the lithosphere and the deep mantle at a point moving at velocity, v, is simply:

$$L = v \cdot T \tag{3}$$

with $T = 15$ my, being the time elapsed.

In fact, all laws can be expressed as a function of the finite displacements, L, and any different hypothesis on T can be accounted for by simply correcting L in proportion to the change in T.

4.2. Numerical and experimental data on LPO and anisotropy

Experimental data on LPOs in olivine aggregates, as well as textural analysis of naturally deformed peridotites, indicate that the crystallographic axes of olivine minerals are strongly reoriented during deformation [17,37–39]. The [100] axes tend to cluster tightly around the stretching lineation (X), and the [010] axes tend to become perpendicular to the foliation plane. The [001] axes are more loosely grouped around the Y direction. At small strains ($\gamma < 1.5$), the distribution of crystallographic axes is generally observed to tighten as deformation increases, leading

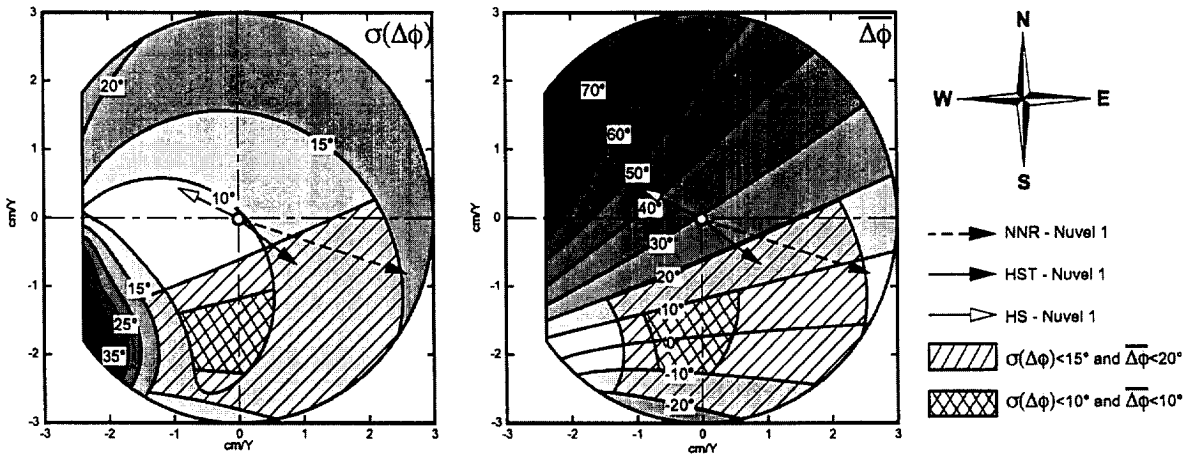

Fig. 4. Mean value, $\Delta\phi$, and standard deviation, $\sigma(\Delta\phi)$, of the difference in the azimuth between SKS fast polarizations reported by McNamara et al. [1] and the direction of block motion relative to deep mantle. A wide range of possible motions for Eurasia, with respect to deep Tibetan mantle, is explored, between 0 and 3 cm/yr in rate, and 0° and 360°E in azimuth. White circle at origin corresponds to Eurasia fixed with respect to deep Tibetan mantle. As also shown in Fig. 3A, this solution yields lithosphere/deep mantle motion differing from SKS fast polarization azimuth by 29°, with 10° standard deviation. Three other solutions from different APM models are also indicated: the no net rotation model of Argus and Gordon [32]; HS-Nuvel 1 from Gripp and Gordon [33]; and HST-Nuvel 1 from Ricard et al. [34]. Th domain in which fast polarization directions and APM motion can be considered in good agreement is defined by $\Delta\phi < 20°$ and $\sigma(\Delta\phi) < 15°$. The best solution would require 2 cm/yr of southward motion of Eurasia with respect to deep mantle beneath Tibet.

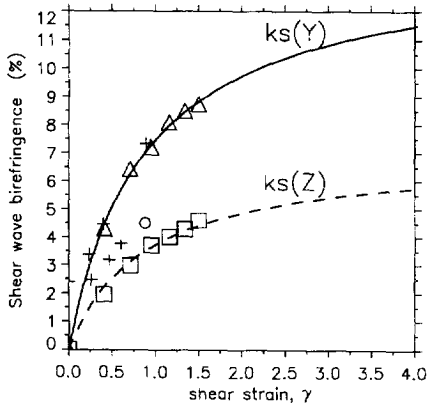

Fig. 5. Birefringence as function of shear strain according to experimental data [37] and deduced from numerical simulations [41]. Experimental data from dunites deformed in axial compression are plotted in equivalent shear strain. + = olivine agregate anisotropy; ○ = neoblast anisotropy after dynamic recrystallisation. Triangles and squares have been computed from the Fisher distributions given in Table 3. They correspond to the splitting of a shear waves propagating respectively in the Y and Z directions. The solid and dashed curves correspond to Eqs. (5 NO TRANSLATION 4), respectively.

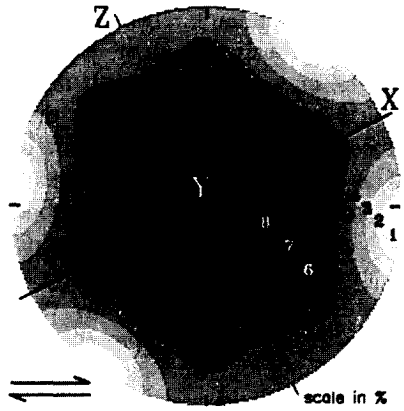

Fig. 6. Shear wave birefringence ($ks = \Delta Vs / Vs$ (%)) for a deformed olivine agregate in simple shear ($\gamma = 1.5$). Olivine minerals are assumed to be distributed according to Fisher distribution, yielding concentration factors of crystallographic axes equivalent to those of Ribe and Yu [41] (Table 3). Dark line indicates the foliation plane (XY). Arrows indicate sense of shear. Equal area diagram.

to a gradual increase in seismic anisotropy. Laboratory experiments [37,40] and numerical simulations [39,41,42] have attempted to quantify this evolution. Experimental measurements compare well with the numerical simulations of Ribe and Yu [41] (Fig. 5). Such distributions can be approximately matched assuming a Fisher distribution of olivine minerals axes (Table 3). In order to obtain some estimate of the seismic anisotropy corresponding to these distributions, we have followed the procedure proposed by Mainprice and Silver [14]. We considered Fisher distributions of single olivine crystal tensors [43], and computed the Voigt average tensor. The birefringence, $ks = \Delta Vs / Vs$, for any direction of propagation of a S wave, is then computed from the elastic wave equation (Christoffel equation) corresponding to this elasticity tensor. Fig. 6 shows how birefringence varies as a function of shear wave propagation direction for a simple shear with $\gamma = 1.5$. Such a pattern compares well with experimental data (see,

Table 3
Simulated LPO as a function of shear strain, γ, (from [41]) compared with LPO obtained assuming a Fisher distribution of olivine mineral tensors

Strain	Ribe and Yu's simulation [41]			Fisher's distribution of Euler angles (°)			Estimated concentration factor		
γ	χ [100]	χ [010]	χ [001]	σ(θ)	σ(φ)	σ(ψ)	χ [100]	χ [010]	χ [001]
0.00	1.00	1.00	1.00	+ ∞	+ ∞	+ ∞	1.00	1.00	1.00
0.41	1.38	1.24	1.01	50	55	50	1.37	1.24	0.96
0.71	1.71	1.41	1.06	38	46	42	1.71	1.39	1.01
0.95	1.97	1.53	1.12	37	41	35	1.99	1.54	1.08
1.16	2.16	1.62	1.16	32	39	37	2.14	1.63	1.12
1.34	2.31	1.71	1.20	31	37	35	2.32	1.73	1.18
1.50	2.48	1.78	1.24	30	37	33	2.54	1.74	1.21

e.g., [14]). The maximum birefringence, about 8.7%, is found for a propagation along Y. The birefringence in the Z direction is about half that maximum value. Values of the birefringence in the Z and Y directions calculated with this procedure are plotted in Fig. 5 as a function of shear strain. Given that foliation planes tend to become horizontal during horizontal shear and that birefringence varies smoothly around the Z direction, we neglect the dip of the foliation planes and consider that birefringence in the Z direction is representative of SKS shear wave splitting.

Numerical simulations indicate that, at strains larger than about $\gamma = 1.5$, intracrystalline slip tends to disorganize the LPO [42,44]. This geometric hardening effect might lead to a decrease in the anisotropy. This process, however, is probably compensated by dynamic recrystallisation, which leads to the growth of grains or newly formed grains (neoblasts) with structures favourably oriented in the strain field [37,40]. Although neoblasts within host grains do not enhance the total LPO, the dynamic recrystallisation probably prevents hardening and keeps the LPO near steady state during uniform simple shear, leading to asymptotic behaviour. Diffusion processes might play a similar role when conditions are such that dislocation creep is still dominant [45,46].

We searched for a simple analytical law that would account both for the experimental data and numerical simulations at strains smaller than 1.5, and for the asymptotic behaviour at larger strain. Given that ophiolitic peridotites that have experienced very large strain are observed to yield S wave seismic anisotropy as large as 13% [14], we set the asymptotic value to 14%. The following equation provides a reasonable fit to the maximum birefringence (Fig. 5):

$$ks(Y) = \Delta Vs/Vs = 0.14(\gamma/(\gamma + 0.88)) \quad (4)$$

with the anisotropy in the Z direction being approximately half the maximum birefringence:

$$ks(Z) = \Delta Vs/Vs = 0.07(\gamma/(\gamma + 0.88)) \quad (5)$$

This latter equation implies an upper asymptotic limit of 7%. For comparison, 5.3% anisotropy in the Z direction has been measured on asthenospheric sample by Mainprice et al. [26]. Eqs. (4 NO TRANSLATION 5) would apply to a pure olivine aggregate, however. Since upper mantle rocks are generally considered to contain 30–40% of other minerals, which tend to develop smaller LPO during strain, a degrading factor should be introduced in these equations in order to apply them to real asthenospheric rocks. On the other hand, numerical

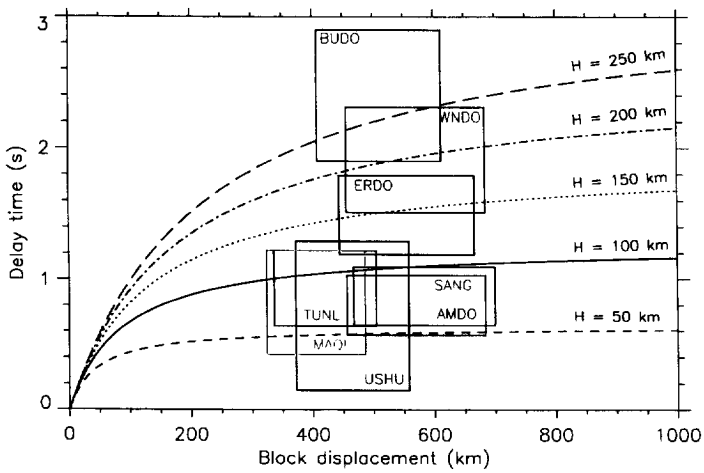

Fig. 7. Relationship between block displacements, L, and delay time, δt. Solid lines represent predicted delay times, according to Eq. (6), for thicknesses of the anisotropic layer varying between 50 and 250 km. Boxes indicate 1σ confidence intervals on δt and block displacements. Uncertainties on block displacements only include uncertainties on Eulerian poles and velocities of Table 1. The present-day kinematics are assumed for the last 15 my. If differential motion of the Eurasian plate with respect to fixed mantle below Tibet were considered, or if the characteristic time span is not 15 my, the boxes should be translated horizontally.

simulations by Wenk et al. [42] have shown that olivine grains in a mixed aggregate with 70% olivine–30% enstatite may develop a stronger LPO than pure olivine aggregates. Similarly, Mainprice and Silver [14] have found that S wave anisotropy is weakly affected by the presence of orthopyroxene in kimberlitic peridotites and that the maximum anisotropy of a 70% olivine–30% orthopyroxene aggregate is only degraded by a factor of 0.8–0.9. We chose to apply a degrading factor of 0.85, which predicts an asymptotic upper limit of 6% in the Z direction, still in agreement with experimental data.

Using Eq. (2) we can derive a simple expression for the predicted delay times due to asthenospheric anisotropy. Eq. (1) can then be expressed as a function of the thickness of the layer, H, and of the amount of finite displacement of the overlying lithosphere relative to the deep mantle, L:

$$\delta t = ks^{*} H/Vs = [0.06^{*} H^{*} L]/[Vs(L + 0.88^{*} H)] \quad (6)$$

As we assumed horizontal foliation planes, this equation might yield slightly overestimated delay times at small strains. In addition, a variable viscosity with depth would lead to heterogeneous strain distribution with systematically smaller cumulative anisotropy than in the hypothesis of a constant viscosity. Our assumptions thus probably provide an upper bound of the delay time that can be expected for a given thickness of the anisotropic layer.

4.3. Discussion

Fig. 7 shows observed delay times at the stations of McNamara et al. [1] as a function of cumulative displacements of the lithosphere, assuming that the kinematics of tectonic deformation has not changed over the last 15 my. The curves indicate predicted delay times according to Eq. (6) for different thicknesses of the anisotropic layer. The observed delay times at the 5 stations located within south central Tibet (AMDO and SANG) and in eastern Tibet (MAQI, USHU and TUNL) would be consistent with a 50–100 km thick, low viscosity layer. Such a thickness compares well with the > 90 km thick Low Velocity Zone evidenced from multiple ScS reverberations along Tibetan paths [47]. As already pointed out by McNamara et al. [1], the larger delay times at the three remaining stations, WNDO, ERDO and BUDO, would imply a much thicker anisotropic layer. If the delay times are interpreted as coming from a single, horizontally sheared layer, a thickness of about 200 km beneath WNDO and ERDO and in excess of 250 km beneath BUDO would be required. The particularly large delay time at BUDO, together with the fault-parallel direction of polarization, may actually be taken to indicate a lithospheric contribution to the total anisotropy, consistent with its location close to the left-lateral Kunlun fault [3]. The crustal anisotropy parallel to the fault strike is further evidence for a lithospheric scale anisotropic layer along the Kunlun fault [13]. Although the Tibetan lithosphere is generally considered to be thin, the lithospheric contribution could be significant because the LPO is favourably oriented to produce maximum birefringence for SKS waves (propagation in the Y direction). The total lithospheric contribution could be larger than 1 s, including a 0.2–0.3 s crustal contribution [13]. Given that the azimuth of the Kunlun fault is close to the direction of tectonic transport, lithospheric and asthenospheric anisotropy might interfere constructively. A particularly thick anisotropic layer in the asthenosphere would nevertheless be required in north-central Tibet, since little contribution from lithospheric anisotropy is expected beneath WNDO and ERDO. This is actually the area where a hot upper mantle has been inferred from various seismological evidence [48–50]. Although we neglected that effect in our modelling, the development of anisotropy depends on the geotherm. Higher temperatures can induce enhanced anisotropy, due to the activation of glide systems such as (010)[100] and (001)[100] [51,52]. This is valid for temperatures between 800°C and 1200°C, so that asthenospheric anisotropy is probably not very sensitive to that effect. Another effect is that the thickness of the anisotropic layer might vary as a function of the geotherm. First, with higher temperatures, the top of the low viscosity zone should tend to reach shallower depths. At the same time, the bottom of the anisotropic layer should get deeper. In fact, the bottom of the anisotropic layer is either the bottom of sublithospheric decoupling layer (which has been our assumption up to now), or the transition depth from predominantly dislocation to diffusion deforma-

tion processes. Diffusion processes are thought to inhibit the development of a strong anisotropy and the transition depth tends to get deeper with higher temperatures [46]. In both hypotheses, a hot upper mantle might, therefore, induce some thickening of the anisotropic layer.

Finally, given the rapid increase in anisotropy at small strains and the asymptotic behaviour at large strain, estimations of the thickness of the asthenospheric anisotropic layer are not too sensitive to the uncertainties on the displacement of the lithospheric blocks with respect to the deep mantle. The observed delay times beneath north-central Tibet can be accounted for with a 200 km thick anisotropic layer, assuming that the kinematics proposed by Avouac and Tapponnier [27] have been proceeding for 10 my or more (corresponds to $L > 400$ km in Fig. 7).

5. Conclusion

The recent measurements of shear waves splitting beneath Tibet offer an exceptional opportunity to investigate the relationship between seismic anisotropy and active tectonic processes in a continental area. Close to the major strike-slip fault zones the anisotropy implies that such faults probably extend into the lithospheric mantle. Although uncertainties are large, the overall pattern of seismic anisotropy away from those faults is consistent with horizontal shear in an asthenospheric layer beneath the extruded Tibetan lithosphere. Seismic anisotropy correlates with regional tectonics if the deep mantle beneath Tibet is assumed to move northward at about 2 cm/yr relative to stable Eurasia. The observed delay times would require that layer to be about 50–100 km thick beneath central Tibet and about 200 km beneath north-central Tibet. The observed anisotropy might have developed over the last 10 my, assuming stationary kinematics of active deformation during that period. The observed anisotropy beneath Tibet therefore seems consistent with rigid blocks that have been undergoing extrusion since the Middle Miocene. In contrast, no information about earlier tectonics is provided. More generally, since the Lattice Preferred Orientation of olivine minerals in the upper mantle evolves rapidly at low strain values and reaches asymptotic behaviour at high strain values, it is probably appropriate, in areas of active continental deformation, to compare seismic anisotropy with the present tectonics.

Acknowledgements

We thank an anonymous reviewer for a useful review and Francis Guillois for having drafted the figures. *[FA]*

References

[1] D.E. McNamara, T.J. Owens, P.G. Silver and F.T. Wu, Shear wave anisotropy beneath the Tibetan Plateau, J. Geophys. Res. 99, 13655–13665, 1994.

[2] A. Hirn, M. Jiang, M. Sapin, J. Diaz, A. Nercessian, Q.T. Lu, J.C. Lepine, D.N. Shi, M. Sachpazi, M.R. Pandey, K. Ma and J. Gallart, Seismic anisotropy as an indicator of mantle flow beneath the Himalayas and Tibet, Nature 375, 571–574, 1995.

[3] J. Guilbert, G. Poupinet and Jiang Mei, A study of azimuthal P-residuals and shear-wave splitting across the Kunlun range (Northern Tibetan Plateau), Phys. Earth Planet. Inter., in press.

[4] L.P. Vinnik, G.L. Kosarev and L.I. Makeyeva, Anisotropy in the lithosphere from the observations of SKS and SKKS, Dokl. Acad. Nauk 278, 1335–1339, 1984 (in Russian).

[5] L.P. Vinnik, L.I. Makeyeva, A. Milev and A.Y. Usenko, Global patterns of azimuthal anisotropy and deformations in the continental mantle, Geophys. J. Int. 111, 433–447, 1992.

[6] P.G. Silver and W.W. Chan, Implications for continental structure and evolution from seismic anisotropy, Nature 335, 34–39, 1988.

[7] P.G. Silver and W.W. Chan, Shear wave splitting and subcontinental mantle deformation, J. Geophys. Res. 96, 16429–16454, 1991.

[8] M.K. Savage and P.G. Silver, Mantle deformation and tectonics: constraints from seismic anisotropy in the Western United States, Phys. Earth Planet. Inter. 78, 207–228, 1993.

[9] V. Babuska, J. Plomerova and J. Sileny, Models of seismic anisotropy in the deep continental lithosphere, Phys. Earth Planet. Inter. 78, 167–191, 1993.

[10] J.P. Montagner and T. Tanimoto, Global anisotropy in the upper mantle inferred from the regionalization of phase velocities, J. Geophys. Res. 95, 4797–4819, 1990.

[11] J.P. Montagner and T. Tanimoto, Goblal upper mantle tomography of seismic velocities and anisotropy, J. Geophys. Res. 96, 20337–20351, 1991.

[12] G. Barruol and D. Mainprice, A quantitative evaluation of the contribution of crustals rocks to the shear wave splitting of teleseismic SKS waves, Phys. Earth Planet. Inter. 78, 281–300, 1993.

[13] G. Herquel, G. Wittlinger and J. Guilbert, Anisotropy and crustal thickness of Northern-Tibet. New constraints for tectonic modelling, Geophys. Res. Lett. 22, 1925–1928, 1995.
[14] D. Mainprice and P.G. Silver, Interpretation of SKS-waves using samples from the subcontinental lithosphere, Phys. Earth Planet. Inter. 78, 257–280, 1993.
[15] J.P. Montagner and D.L. Anderson, Petrological constraints on seismic anisotropy, Phys. Earth Planet. Inter. 54, 82–105, 1989.
[16] N.I. Christensen, The amplitude, symmetry and origin of upper mantle anisotropy based on fabric analyses of ultramafic tectonites, Geophys. J. R. Astron. Soc. 76, 89–111, 1984.
[17] A. Nicolas and N.I. Christensen, Formation of anisotropy in the upper mantle peridotites: a review, in: Composition, Structure and Dynamics of the Lithosphere/Asthenosphere System, K. Fuchs and C. Froidevaux, Eds., pp. 111–123, Am. Geophys. Union, 1987.
[18] P. Molnar and P. Tapponnier, Cenozoic tectonics of Asia: Effects of a continental collision, Science 189, 419–426, 1975.
[19] P. Tapponnier and P. Molnar, Active faulting and tectonics of China, J. Geophys. Res. 82, 2905–2930, 1977.
[20] G. Peltzer and P. Tapponnier, Formation and evolution of strike-slip faults, rifts and basins during the India–Asia collision: an experimental approach, J. Geophys. Res. 93, 15095–15117, 1988.
[21] G.A. Houseman and P. England, Finite strain calculations of continental deformation 2. Comparison with the India–Asia collision zone, J. Geophys. Res. 91, 3664–3676, 1986.
[22] P. England and P. Molnar, Right-lateral shear and rotation as the explanation for strike-slip in eastern Tibet, Nature 344, 140–142, 1990.
[23] C. DeMets, R.G. Gordon, D.F. Argus and S. Stein, Current plate motions, Geophys. J. Int. 101, 425–478, 1990.
[24] G.A. Houseman, D.P. McKenzie and P. Molnar, Convective instability of a thickened boundary layer and its relevance for the thermal evolution of continental convergence belts, J. Geophys. Res. 86, 6115–6132, 1981.
[25] P. Molnar, P. England and J. Martinod, Mantle dynamics, uplift of the Tibetan Plateau, and the Indian Monsoon, Rev. Geophys. 31, 357–396, 1994.
[26] D. Mainprice, P.G. Silver and A. Nicolas, Constraints on the mantle seismic anisotropy from the petrofabrics of mantle samples, 2nd Int. Workshop on Dynamics of the Subcontinental Mantle from Seismic Anisotropy to Mountain Building, La Grande Motte, France, 1994.
[27] R. Armijo, P. Tapponnier and T.L. Han, Late-Cenozoic right-lateral strike-slip faulting in southern Tibet, J. Geophys. Res. 94, 2787–2838, 1989.
[28] J.P. Avouac and P. Tapponnier, Kinematic model of active deformation in Central Asia, Geophys. Res. Lett. 20, 895–898, 1993.
[29] B. Meyer, Mécanismes des grands tremblements de terre et du raccourcissement crustal oblique au bord nord-est du Tibet, Ph.D. Thesis, Univ. Paris VI, 129 pp., 1991.
[30] C.R. Allen, L. Zhuoli, Q. Hong, W. Xueze, Z. Huawei and H. Weishi, Field study of a highly active fault zone: the Xianshuihe fault of southwestern China, Geol. Soc. Am. Bull. 103, 1178–1199, 1991.
[31] W.S.F. Kidd and P. Molnar, Quaternary and active faulting observed on the 1985 Academia–Sinica Royal Society geotraverse of Tibet, Philos. Trans. R. Soc. London Ser. A 327, 337–363, 1988.
[32] D.F. Argus and R.G. Gordon, No-net-rotation model of current plate velocities incorporating plate motion model Nuvel-1, Geophys. Res. Lett. 18, 2039–2042, 1991.
[33] R. Gripp and R.G. Gordon, Current plate velocities relative to the hotspots incorporating the Nuvel-1 global plate motion model, Geophys. Res. Lett. 17, 1109–1112, 1990.
[34] Y. Ricard, C. Doglioni and R. Sabadini, Differential rotation between lithosphere and mantle: a consequence of lateral mantle viscosity variations, J. Geophys. Res. 96, 8407–8415, 1991.
[35] A. Briais, P. Patriat and P. Tapponnier, Updated interpretation of magnetic anomalies and seafloor spreading stages in the south China Sea, J. Geophys. Res. 98, 17757–17771, 1993.
[36] T.M. Harrisson, P. Copeland, W.S.F. Kidd and A. Yin, Raising Tibet, Science 255, 1663–1670, 1992.
[37] A. Nicolas, F. Boudier and A.M. Boullier, Mechanisms of flow in naturally and experimentally deformed peridotites, Am. J. Sci. 273, 853–876, 1973.
[38] A. Nicolas and J.P. Poirier, Crystalline Plasticity and Solid State Flow in Metamorphic Rocks, 444 pp., Wiley, New York, 1976.
[39] A. Etchecopar and G. Vasseur, A 3-D kinematic model of fabric development in polycrystalline aggregates: comparisons with experimental and natural examples, J. Struct. Geol. 9, 705–717, 1987.
[40] H.G. Avé Lallement and N.L. Carter, Syntectonic recrystallisation of olivine and modes flow in the upper mantle, Geol. Soc. Am. Bull. 81, 2203–2223, 1970.
[41] N.M. Ribe and Y. Yu, A theory for plastic deformation and textural evolution of olivine polycrystals, J. Geophys. Res. 96, 8325–8335, 1991.
[42] H.R. Wenk, K. Bennett, G.R. Canova and A. Molinari, Modeling plastic deformation of peridotite with the self consistent theory, J. Geophys. Res. 96, 8337–8349, 1991.
[43] M. Kumazawa and O.L. Anderson, Elastic moduli, pressure derivatives and temperature derivatives of single crystal olivine and single crystal forsterite, J. Geophys. Res. 74, 5961–5980, 1969.
[44] Y.B. Chastel, P.R. Dawson, H.S. Wenk and K. Bennett, Anisotropic convection with implications for the upper mantle, J. Geophys. Res. 98, 17757–17771, 1993.
[45] S. Karato, M.S. Paterson and J.D. Fitz Gerald, Rheology of synthetic olivine aggregates: influence of grain size and water, J. Geophys. Res. 91, 8151–8176, 1986.
[46] S. Karato and P. Wu, Rheology of the upper mantle: a synthesis, Nature 260, 771–777, 1993.
[47] J. Revenaugh and S.A. Sipkin, Mantle discontinuity structure beneath China, J. Geophys. Res. 99, 21911–21927, 1994.
[48] J. Ni and M. Barazangi, High frequency seismic wave propa-

gation beneath the Indian shield, Himalayan arc, Tibetan Plateau, and surrounding regions: High uppermost mantle velocities and efficient Sn propagation beneath Tibet, J. R. Astron. Soc. 72, 665–689, 1983.

[49] P. Molnar and W.P. Chen, S–P wave travel time residuals and lateral inhomogeneity in the mantle beneath Tibet and the Himalaya, J. Geophys. Res. 89, 6911–6917, 1984.

[50] L. Bourjot and B. Romanowicz, Crust and upper mantle tomography in Tibet using surface waves, Geophys. Res. Lett. 19, 881–884, 1992.

[51] N.L. Carter and H.G. Avé Lallemant, High temperature flow of dunite and peridotite, Geol. Soc. Am. Bull. 81, 2181–2202, 1970.

[52] W.B. Durham and C. Goetze, Plastic flow of oriented single crystals of olivine, 1, Mechanical data, J. Geophys. Res. 82, 5737–5753, 1977.